



# Episodic diamond growth beneath the Kaapvaal Craton at Jwaneng Mine, Botswana

Michael U. Gress<sup>1</sup> · Daniel Howell<sup>1,2</sup> · Ingrid L. Chinn<sup>3</sup> · Laura Speich<sup>4</sup> · Simon C. Kohn<sup>4</sup> · Quint van den Heuvel<sup>1</sup> · Ellen Schulten<sup>1</sup> · Anna S. M. Pals<sup>1</sup> · Gareth R. Davies<sup>1</sup>

Received: 27 November 2017 / Accepted: 20 April 2018 / Published online: 24 May 2018  
© The Author(s) 2018

## Abstract

Important implications for the interior workings of the Earth can be drawn by studying diamonds and their inclusions. To better understand the timing and number of diamond forming events beneath the NW margin of the Kaapvaal Craton, a comprehensive reassessment of Jwaneng's diamond populations has been undertaken. We report new inclusion abundance data from the visual examination of ~130,000 diamonds that validate the predominance of an eclogitic diamond suite (up to 88%) with on average 5% inclusion-bearing diamonds (with inclusions >10 µm in size). From this population, polished plates from 79 diamonds of eclogitic and peridotitic paragenesis have been studied with cathodoluminescence (CL) imaging and infrared spectroscopy (FTIR) traverses. The majority (80%) record major changes in N concentration and aggregation states, as well as sharp boundaries in the CL images of individual plates that are interpreted to demarcate discrete diamond growth events. In addition, bulk FTIR data have been acquired for 373 unpolished diamonds. Silicate inclusions sampled from distinct growth zones define 2 compositional groups of omphacites and pyrope-almandines associated with different N contents in their diamond hosts. These findings reinforce previous observations that at Jwaneng at least seven individual diamond forming events can be identified – 3 peridotitic and 4 eclogitic. The results demonstrate that detailed examination of diamond plates by CL imaging and FTIR traverses is necessary to unveil the complex history recorded in diamonds.

**Keywords** Nitrogen aggregation · FTIR · Silicate inclusions · Cathodoluminescence

## Introduction

Diamonds are considered ‘ancient messengers’ from Earth's interior. Inclusions trapped during distinct diamond forming

events provide insight into the temporal tectono-magmatic evolution of the subcontinental lithospheric mantle (SCLM) and the deep carbon cycle. However, the absolute number of diamond-forming events recorded in the mantle beneath an individual diamond mine and the scale of these events, remains unknown. Hence, it is vital to establish the timing of diamond forming events: e.g., by analysing individual sulphide inclusions for Re-Os isochron ages (Pearson et al. 1998; Wiggers de Vries et al. 2013). Initial attempts have also been made to date individual silicate diamond inclusions using the Sm-Nd isochron method e.g., at the Orapa kimberlite cluster in Botswana and at Finsch, Kimberley and Venetia diamond mines, South Africa (Koorneef et al. 2017; Smith et al. 1991; Timmerman et al. 2017). These data indicate multiple temporally-distinct diamond forming events at the same diamond mine. Similar conclusions have been reached in studies of the 240 Ma Jwaneng kimberlites on the NW rim of the Archaean Kaapvaal Craton (Kinny et al. 1989). Based on C and N stable isotope ratios, N concentration and N aggregation state data obtained by Fourier-transform infrared

---

Editorial handling: T. Stachel

---

**Electronic supplementary material** The online version of this article (<https://doi.org/10.1007/s00710-018-0582-y>) contains supplementary material, which is available to authorized users.

---

✉ Michael U. Gress  
m.u.gress@vu.nl

- <sup>1</sup> Vrije Universiteit, De Boelelaan 1085, 1081, HV Amsterdam, The Netherlands
- <sup>2</sup> Department of Earth and Atmospheric Sciences, University of Alberta, Edmonton, AB T6G 2E3, Canada
- <sup>3</sup> De Beers Exploration, Johannesburg, South Africa
- <sup>4</sup> School of Earth Sciences, University of Bristol, Queens Rd, Bristol BS8 1RJ, UK

(FTIR) spectroscopy and major element compositions of inclusions, multiple eclogitic and peridotitic populations have been inferred: the age of eclogitic diamond formation at Jwaneng was previously determined using a 2-point Sm-Nd isochron on composite silicate inclusions and yielded an age of  $1540 \pm 20$  Ma with indication of a second population formed at around 1 Ga (Richardson et al. 1999). Similarly, sulphide inclusions define 2 generations of eclogitic diamonds, one with a Proterozoic (1.5 Ga) age and another suite of Archean (2.9 Ga) age (Richardson et al. 2004; Thomassot et al. 2009). There are no isochron ages available for the peridotitic diamond suite at Jwaneng and only their relative age is constrained based on inclusion chemistry and C-isotope and FTIR data from the diamond hosts (Deines et al. 1997; Stachel et al. 2004). Those FTIR and C-N-isotope data for peridotitic diamonds were acquired on the same fragments but there are no references which part of the diamond (i.e., core or rim) these pieces represent (Cartigny et al. 1998; Deines et al. 1997; Thomassot et al. 2009).

The present study reports a detailed assessment of the diamond populations at Jwaneng to further constrain the number of diamond-forming events beneath an individual mine. New inclusion abundance data from the visual examination of ~130,000 diamonds refine proportions of different inclusion suites. Of these, bulk FTIR data were acquired for 373 whole diamonds, and polished plates from 79 diamonds of eclogitic and peridotitic paragenesis were studied through cathodoluminescence (CL) imaging, with FTIR traverses conducted and major element inclusion data interpreted based on recognised growth zones.

## Samples and methods

Over a 4-year period (2013 to 2017) run of mine production was examined from Jwaneng Mine (north, centre and south pipes) with diamonds ranging in size from 0.1 to 0.8 carat (Diamond Trading Company (DTC) sieve classes +07, +09, +11, and 3 grainers) at the Diamond Trading Company in Gaborone, Botswana (DTCB). In total, over 130,000 diamonds were characterised visually for their inclusion content using a binocular microscope. Inclusions were defined as recognisable minerals >10  $\mu\text{m}$  in size. The main distinction criterion is based on differences in colour between, e.g., eclogitic pyrope-almandine garnet (orange), omphacitic clinopyroxene (cpx; pale green) and kyanite (blue) inclusions and peridotitic pyrope garnet (purple), olivine or orthopyroxene (yellow to colourless) and chromite (brown to black) inclusions. Sulphide inclusions were almost ubiquitously associated with a characteristic rosette fracture system around the inclusion. If not otherwise reported, the examined diamonds are of gem and near-gem quality.

Sample selection concentrated on diamonds containing multiple large (>50  $\mu\text{m}$ ) garnet, clinopyroxene and sulphide inclusions. After morphological characterization, 79 diamond plates of eclogitic (69) and peridotitic (8) paragenesis, as well as 2 sulphide-bearing diamonds were laser cut through the centre of the diamond along the (110) plane to produce plates of 0.3 to 1.8 mm thickness, followed by surface polishing on a cast iron scaife plate. The polished plates were photographed on a Nikon SMZ1500 microscope using its extended depth of focus (EDF) imaging software. Cathodoluminescence imaging was performed on the uncoated diamond plates on a Cambridge Image Technology Ltd. cold cathode luminescence 8200 mk3 instrument (attached to an optical microscope) operating with an acceleration voltage of 10 kV, a beam current of 400  $\mu\text{A}$  and camera exposure times between 1 to 15 s.

Infrared absorbance spectra were collected on a number of instruments with different experimental settings. Bulk spectra of 373 randomly sampled diamonds from Jwaneng run-of-mine production (DTC +09 gem and near-gem) were measured using Perkin Elmer and Bruker Alpha spectrometers during the sampling campaigns at DTCB. Spectra comprised 10 scans over the range 4000 to 400  $\text{cm}^{-1}$  with a resolution of 8  $\text{cm}^{-1}$ .

Based on observations from the CL imaging, FTIR traverses were acquired from representative parts of the central plates. The majority of the plate analyses were performed using a FT/IR Jasco-470+ instrument equipped with a Jasco Irttron IRT-30 infrared microscope over the spectral range 4000 to 650  $\text{cm}^{-1}$  with a resolution of 4  $\text{cm}^{-1}$ . The remaining plate analyses were performed using either a Thermo-Nicolet Nexus spectrometer attached to a continuum infrared microscope (4  $\text{cm}^{-1}$  resolution) or a Thermo Nicolet iN10MX infrared microscope (2  $\text{cm}^{-1}$  resolution). Depending on the thickness of the plate, the aperture was set between 50 to 100  $\mu\text{m}$ . After background acquisition prior to every sample measurement, 5 to 20 spots were measured from core to rim on each plate.

All spectra were processed using the automated version of DiaMap (Howell et al. 2012a, b) to determine N content and aggregation state. The data collected using the Thermo Nicolet iN10MX were also processed using a Python program (Kohn et al. 2016; Speich et al. 2017). Given that both programs use a similar approach for N deconvolution (normalisation, subtraction of a Type IIa diamond spectrum, fitting of N components while adding a linear correction), they produced data in good agreement. Spectra with <50 atomic ppm (at.ppm) N were reprocessed manually using the Excel version of DiaMap, to provide greater confidence in reported values. Nitrogen concentrations were calculated from absorption coefficients at 1282  $\text{cm}^{-1}$ :  $[\text{NA}] = 16.5$  ppm (Boyd et al. 1994) and  $[\text{NB}] = 79.4$  ppm (Boyd et al. 1995). Errors for N content and N aggregation (expressed as  $\%B = 100B/[A + B]$ )

are typically  $\pm 10\%$  and  $\pm 5\%$ , respectively, but uncertainties increase with plate thickness (see Kohn et al. (2016) for more details) and the size of the aperture, especially for spectra recording low N contents ( $< 50$  at.ppm). In particular, it should be noted that if spectra of heterogeneous, zoned diamonds are collected using whole diamonds or thick plates it is likely that the analysed volume will contain diamond with variable N concentrations. If this is the case, the measured N will be the average within the analysed volume, but the N aggregation will be heavily weighted towards the high N regions (Kohn et al. 2016). Furthermore, the ‘points’ measured by FTIR of diamond plates do not correspond exactly with the zoning elucidated by CL that shows near-surface features of the plate, whereas FTIR absorption represents a conical volume through the sample. This is particularly important if data points from the transects are close to growth zone boundaries, resulting in spectra that reflect contributions from more than one growth zone. Hence, sampling points were positioned to avoid clear boundaries between growth zones.

Given the low spectral resolution at which some bulk analyses were performed, it is not always possible to accurately differentiate low N samples from those typically deemed as ‘nitrogen-free’ (Type II). The present study considers all measurements with  $< 20$  at.ppm N as ‘nitrogen below detection limit’. Since the diamonds show no blue colouration and B-centre related absorption in FTIR spectra these spectra are classified as ‘Type IIa’.

For a subset of samples encapsulated inclusions were liberated from the plates and off-cuts using a steel crusher. Single inclusions will be measured for Sm-Nd geochronology in the future, so inclusions were not polished before analysis to avoid sample loss. Garnet (gnt) and cpx inclusions were mounted on carbon tape and a horizontal surface used for electron microprobe analyses. The EMPA analyses were performed using a JEOL JXA-8350F instrument with an acceleration voltage of 15 kV, a beam current of 25 nA and a beam size of 1  $\mu\text{m}$  at Utrecht University. The CITZAF correction method was applied to the raw data. Further analytical details follow the protocol of Timmerman et al. (2015) that stipulates normalization of the data to 100% and only includes measurements within 2 standard deviations of the mean. The normalisation of the major element data, which is based on average compositions of individual analyses ( $n = 3$  to 22) with totals from 92 to 100 wt%, allows direct comparison of the inclusion compositions.

## Results

### Relative proportions of inclusion suites

On average, 5% of the diamonds at Jwaneng contain inclusions (Table 1). Sulphide inclusions are the most abundant (~

63%, Fig. 1). Diamonds containing multiple sulphides are more abundant but the sulphides are smaller in size compared to diamonds containing single sulphide inclusions. A visual distinction between eclogitic and peridotitic sulphide inclusions was only possible when silicate inclusions were also present in the diamond, and diamonds with combined eclogitic silicate and sulphide inclusions account for ~5% of the inclusion-bearing diamonds. Eclogitic inclusions dominate the silicate population, averaging 69% (Table 1). Six percent of inclusions were unidentified silicates, 6% contained P-type silicate inclusions (Fig. 1),  $< 0.1\%$  had combined peridotitic silicate/ sulphide inclusions. A detailed overview of the 15 individual production parcels examined for relative inclusion proportions can be found in the Online Resources (ESM 1).

### Diamond morphology

Polished plates were mainly prepared from octahedral to dodecahedral diamonds, but irregular shapes and macles were also present. Surface features show resorption, stepped faces and trigons. The majority of these diamonds were colourless but some diamonds with different shades of yellow and brown, 2 green coated (from radiation staining) and one pink diamond were also present. Further details are presented in the Online Resources (ESM 2).

### CL imaging

Cathodoluminescence imaging of the central plates (Fig. 2) reveals growth histories of the individual diamonds ranging from a single well-defined growth zone (Fig. 2b) to samples having multiple (2 to 4+) growth zones that are recognized by sharp, successive boundaries (Fig. 2e–i). A growth zone may be compromised of multiple similar (genetically related) growth layers. In contrast, resorption horizons show irregular geometry (Fig. 2d core) and can be difficult to distinguish from superimposition of different growth directions (Fig. 2f intermediate zone), especially when successive precipitation of growth layers was involved in diamond formation (Fig. 2f, k). A resorption horizon can also represent a surface for a new growth zone (Fig. 2l intermediate zone).

### FTIR analyses of bulk diamonds

Nitrogen content and aggregation states of bulk (unpolished) diamonds within each of the 3-studied production parcels ranges from N below detection limit ( $< 20$  at.ppm) to 1466 at.ppm N and 0 to 100 %B, respectively (Fig. 3). Nine diamonds are pure Type IaA, 17 are Type IaB, 4 are Type IIa, the remaining are all Type IaAB (i.e. 10–90 %B) as listed in the Online Resources (Table ESM 3).

**Table 1** Relative inclusion proportions in diamonds at Jwaneng

DTC sieve class	Diamonds	Silicates [%]			Sulphides [%]		Eclogitic silicates and sulphides [%]	Eclogitic inclusions* [%]	Total inclusions** [%]
		E	P	UN	Single	Multiple			
+07	27,500	23.1	6.1	6.9	24.4	29.2	10.4	72.0	4.6
+09	48,800	18.3	5.6	5.3	28.0	39.4	3.4	66.7	5.2
+11	37,700	21.1	6.5	5.9	23.2	39.6	3.7	66.7	5.1
3Gr	10,300	27.1	7.0	6.7	33.1	42.0	6.4	70.9	4.3
Total	130,000	20.4	5.7	5.8	25.9	37.3	4.8	68.7	5.0

Details on the proportions of individual production lots can be found in the Online Resource (ESM 1)

E, eclogitic inclusions; P, peridotitic inclusions; UN, unidentified silicate

\*Percentage of eclogitic inclusions calculated from eclogitic silicates plus combined eclogitic silicates and sulphides over the total number of silicate and combined eclogitic silicate and sulphide inclusions

\*\*Percentage of total amount of inclusions calculated by total number of inclusions over number of diamonds

### FTIR analyses of central plates

The majority of the diamond plates are Type IaAB (51), one diamond (JW407) is Type IaA, 17 have Type IIa growth zones but also record detectable N (>20 at.ppm) in at least one other major growth zone (Fig. 2h–j), 12 diamonds are entirely Type IIa (Fig. 2a). Together with insights from the CL imaging, each plate was subdivided into distinct growth zones (i.e., core, intermediate, rim) where N contents showed a variation >100 at.ppm between individual FTIR analyses as listed in the Online resources (Table ESM 4). Further, the plates were classified into 4 main groups: (A) *Type IIa* (15%; 10 E-, 2 P-types) as described above; (B) showing *homogeneous growth* with fairly constant N content and aggregation (3%; 1 E- & 1 P-type); (C) *systematic changes* in N content from core to rim with (C1) *increasing* (25%; 19 E-, 1 S-type), (C2) *decreasing* (38%; 25 E-, 4 P-, 1 S-types) and (C3) *increasing and decreasing* (16%; 12 E- & 1 P-type) between individual growth zones; and (D) showing *non-systematic variations* (3%; 2 E-types) in N content and aggregation state associated with irregular growth, possibly relating to plates not cut through the growth centre in some cases.

Individual eclogitic diamonds of *group C* (>80% of all studied diamond plates) record 2 (e.g., JW047, JW111; Fig. 2h, e), 3 (e.g., JW024, JW060; Fig. 2g, k) or 4 (e.g., JW033, JW194; Fig. 2d, l) distinct growth zones. *Group C* peridotitic diamonds have 2 (JW243; Fig. 2j) or 3 (JW083, JW089, JW102; Fig. 2i) distinct growth zones. Further transects of N content and aggregation state of the remaining 79 diamond plates are provided in the Online Resources (ESM 5).

Nitrogen content and aggregation state recorded in traverses range from N below detection limit to 1368 at.ppm N and 0 to 100 %B. These data cover most of the range of previously reported N contents (up to 1990 at.ppm N) and aggregation data for Jwaneng (Deines et al. 1997; Thomassot et al. 2009). The range of N contents and

aggregation states within individual diamonds is, however, larger in the present dataset. In sample JW141, the N content varies from 1070 at.ppm in the core to 90 at.ppm in the intermediate zone and 400 at.ppm in the rim, while in JW351, the aggregation varies from 97 %B in the core to 2 %B in the rim. This compares with previous data that reported maximum differences of 216 at.ppm (Cartigny et al. 1998) and 402 at.ppm and 28% in JW0020 (Thomassot et al. 2009).

Deines et al. (1997) proposed that the N aggregation characteristics in their sample population (cleaved diamond chips,  $n = 68$ ) formed 2 groups (0–10 %B; 50–70 %B). These groups are not observed in either the bulk or plate data presented here. Only a single peak at ~95%B for the plate data is observed (see Online Resources ESM 6).

### Modelled mantle residence temperatures

The N aggregation state of a diamond in the mantle varies strongly with residence temperature (and to a lesser extent with time) and therefore can be used to obtain insight into a diamond's thermal history. If the approximate formation time of a diamond (or a distinct growth layer) is known, a time averaged residence temperature can be calculated (Leahy and Taylor 1997).

Temperatures modelled for the FTIR data of plates and bulk diamonds in Fig. 3 were calculated for diamond genesis at 1, 1.5 and 2.9 Ga and kimberlite eruption at 240 Ma, based on ages reported in the literature (Richardson et al. 1999, 2004). Assuming diamond formation at 1540 Ma, mantle residence temperatures of bulk diamonds and the plates vary from ~1010 to >1250 °C. Some plates (Fig. 3) have a relatively homogeneous temperature record (JW020, JW083, JW407), while others seem to reflect a gradual shift (e.g., JW024, JW044, JW102) that in some cases might not be beyond the uncertainty in the data (e.g. JW044). In contrast, other examples imply distinct changes of up to several tens



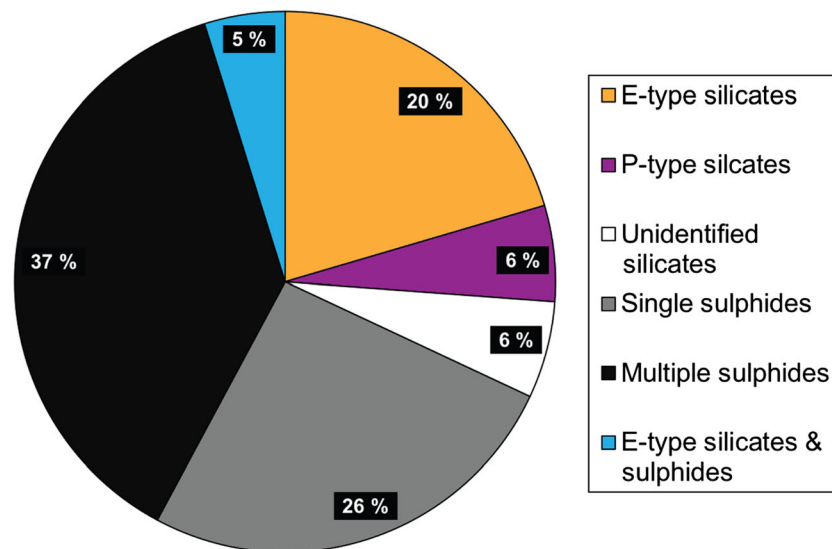


**Fig. 1** Average relative proportions of inclusions in the run of mine production of the Jwaneng mine, Botswana. The inclusions are subdivided into eclogitic (E), peridotitic (P) and unidentified silicates; single and multiple sulphides; and eclogitic sulphides and silicates. Inclusions were defined as recognisable minerals (>10  $\mu\text{m}$ ) for counting purposes; in total ~130,000 diamonds were examined. The

of degrees between individual growth zones that cut across isotherms (e.g., JW033, JW060, JW114, JW147, JW175, JW194). Overall, the FTIR data of the plates (Fig. 3) show a clustering of diamond cores at higher N aggregation (70 to 90 %B; ~1200 to 1250  $^{\circ}\text{C}$  for all 3 calculated ages) and to a lesser extent of lower aggregation states (10 to 30 %B; ~1050 to 1150  $^{\circ}\text{C}$ ), where also the majority of rims is located. Data from intermediate growth zones span the whole range. It should be noted that if the analysed volume is not homogeneous in N concentration (which is certain to be the case for most bulk diamonds and some points from traverses on plates), there will be a systematic and predictable overestimate of the mantle residence temperatures (Kohn et al. 2016) that may have some effect on the distribution of the FTIR data in Fig. 3.

## Inclusion compositions

### General remarks

Inclusion compositional data are summarized in Table 2 for 30 omphacite and 15 pyrope-almandine inclusions liberated from 16 diamonds. All omphacite inclusions (Fig. 4a) are characterised by moderate molar Mg# (71 to 87) and low molar Cr# (<5). Pyrope-almandine inclusions (Fig. 4b) have low  $\text{Cr}_2\text{O}_3$  (0.5 wt%) with CaO between 4 and 14 wt%. These compositions fall in the eclogite (G4 and G5) garnet fields as defined by Grütter et al. (2004) and are comparable with previous studies of Jwaneng inclusions (Richardson et al. 1999; Richardson et al. 2004; Stachel et al. 2004). The compositional variation between inclusions, liberated from the same

inclusion abundance varies between diamond size fractions that ranged from 0.1 to 0.8 carat (sieve class +7 to 3 grainers) and averaged 5% at Jwaneng. Note that ~99% of diamonds containing both silicate and sulphide inclusions are of eclogitic paragenesis. Hence, up to 88% of all inclusion-bearing diamonds at Jwaneng are inferred to be eclogitic

diamond, is between zero to 2.3 wt% in CaO and < 0.3 wt% in  $\text{Cr}_2\text{O}_3$  for garnet and between 0.3 to 5.6 in Mg# and < 0.7 in Cr# for cpx.

### Coupled diamond-inclusion relationships

The omphacite inclusions define 2 subgroups with (1) low-Mg# (71 to 83) and low-Cr# from 0.2 to 1.4 (JW030, JW101, JW111, JW137, JW138, JW147, JW194) from diamond growth zones with  $\geq 50$  to 700 at.ppm N, and (2) omphacite inclusions with high-Mg# (79 to 87) and high-Cr# from 2.8 to 4.7 from diamond growth zones having  $\leq 50$  at.ppm (JW048, JW058, JW070, JW080, JW112, JW116, JW124). The majority of low-Ca (3.8 to 6.1 wt% CaO) pyrope-almandine inclusions (JW058, JW137, JW147 core) are from growth zones characterized by  $\leq 50$  at.ppm N (Fig. 4b), only JW175 shows high N contents (~1000 at.ppm). The pyrope-almandine inclusions (JW068, JW147 intermediate, JW194) from diamond growth zones with N contents from 50 to 300 at.ppm are all characterised by high CaO contents (7.9 to 13.5 wt%).

## Discussion

### Inclusion abundance

The average proportion of inclusion-bearing diamonds for 130,000 Jwaneng diamonds, comprising DTC sieve sizes +7, +9, +11, and 3 grainers (equivalent to a combined range from 0.1 to 0.8 carats), is 5%. Previous studies of inclusion-

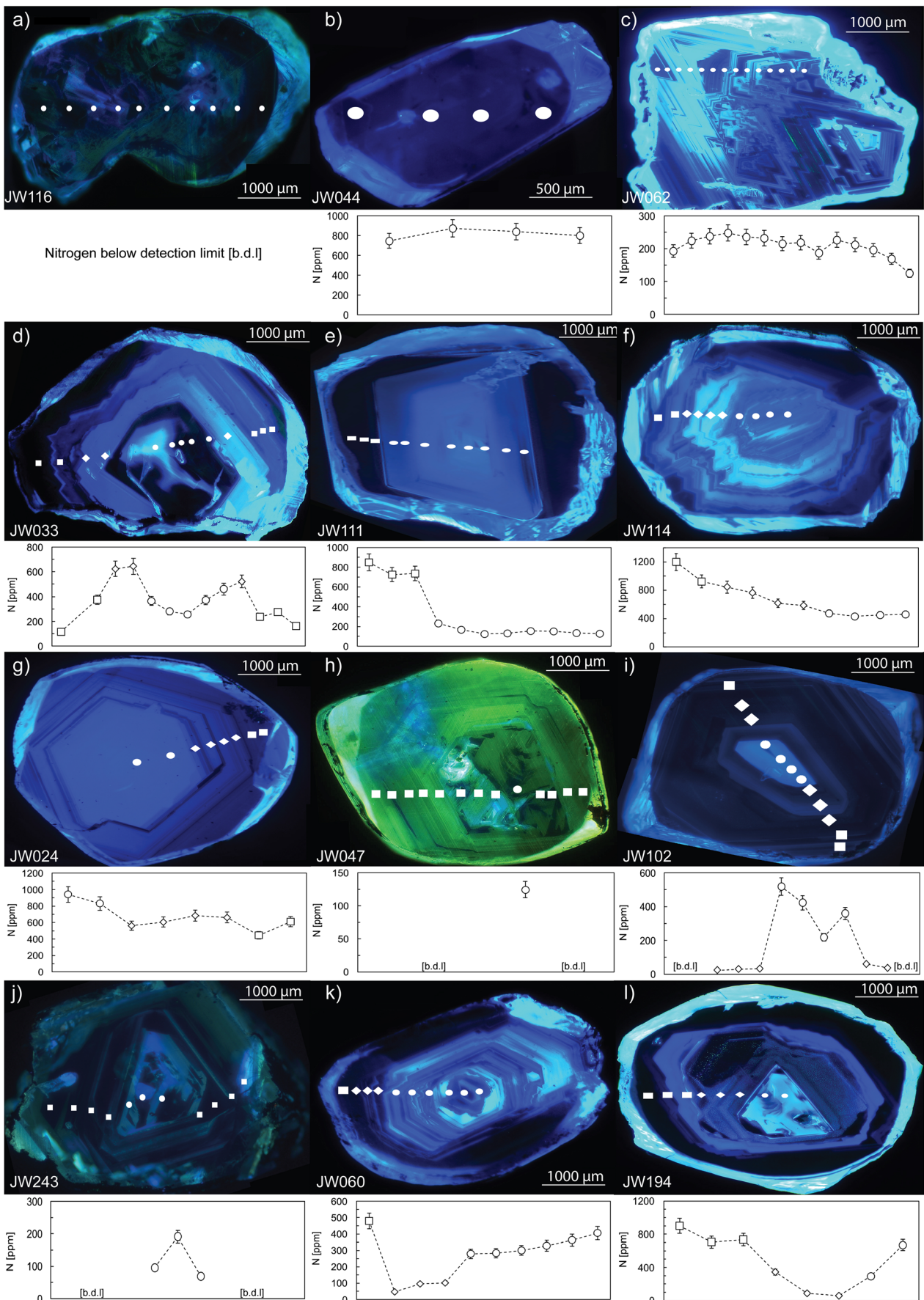


**Fig. 2** Cathodoluminescence images and N traverses of representative polished plates. The diamonds illustrate common growth features (in groups A to D defined in the text) with samples **a**) JW116 (A), **b**) JW044 (B), **c**) JW062 (D), **d**) JW033 (C1), **e**) JW111 (C1), **f**) JW114 (C1), **g**) JW024 (C2), **h**) JW047 (C2), **i**) JW102 (C2), **j**) JW243 (C2), **k**) JW060 (C3) and **l**) JW194 (C3). White symbols correspond to the location where FTIR spectra were acquired and are subdivided into major growth zones: core (filled circles), intermediate (diamonds) and rim (squares). Type IIa spectra (<20 at.ppm N) are marked as below detection limit (b.d.l.)

bearing diamonds at Jwaneng report 0.7% from 127,000 diamonds of DTC sieve size +05 (Stachel and Harris 2008). A possible explanation for the different abundance data can be differences in sampling criteria (e.g., different inclusion size cut off) and the overall time of the campaign (sampling of different kimberlite facies and varying input of the 3 pipes). Based on the observation of associated silicate and oxide inclusions, over 99% of sulphide inclusions are thought to be of eclogitic paragenesis and hence, at least 88% of all inclusion-bearing diamonds at Jwaneng are eclogitic. Only 6% of inclusions are unambiguously assigned to a peridotitic assemblage while the paragenesis of the remaining 6% of inclusions could not be identified (Fig. 1).

A general predominance of the eclogitic inclusion suite for Jwaneng (Table 1) was also noted in previous studies (Gurney et al. 1995). Stachel et al. (2004) and references therein link the eclogitic predominance to Proterozoic magmatic and tectonic events that triggered eclogitic diamond formation, potentially resorbing parts of any pre-existing peridotitic diamond suite.

## Growth characteristics

### General remarks

Studies of diamond populations worldwide almost always reveal variations in colour and morphology (Gurney et al. 2004). Deines et al. (1997) suggested a rough classification of Jwaneng diamonds based upon their colour, morphology and paragenesis. They concluded E-type diamonds were more often colourless, partially resorbed and of irregular shape, compared to the P-type diamonds that were more commonly octahedral and green coated or brown and deformed. No coherent relationships were reported between N characteristics and diamond paragenesis. The same lack of relationship is observed in the present dataset. While bulk FTIR analyses in

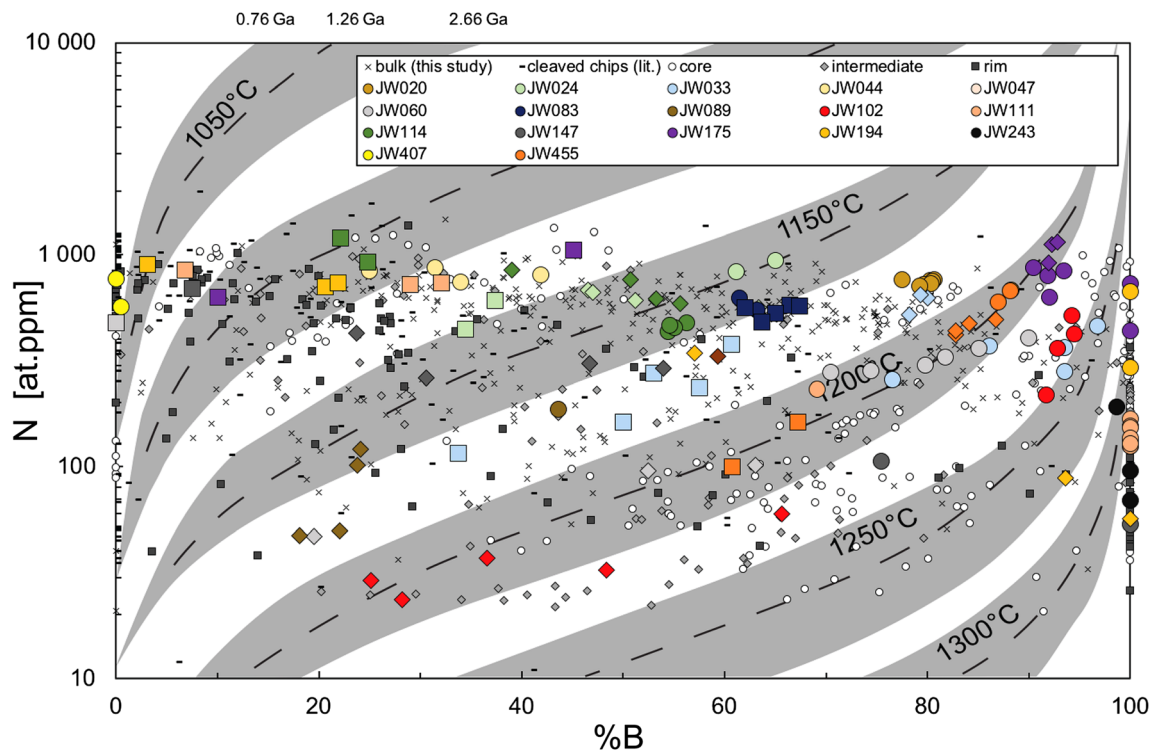


**Fig. 3** Nitrogen content plotted against N aggregation for diamond plates, bulk diamonds and literature data from Jwaneng. Nitrogen content (at.ppm) in log scale; N aggregation is expressed as the relative proportion of N in fully aggregated B centres (%B) for the studied diamond plates, 373 analyses of bulk diamonds, and literature data (for cleaved chips or fragments) from Deines et al. (1997), Cartigny et al. (1998) and Thomassot et al. (2009). Note: only data with >20 at.ppm N

were plotted. Isotherms for assumed mantle residence times (calculated after Leahy and Taylor (1997)) of 2.66, 1.26 and 0.76 billion years are based on diamond formation at 2.9, 1.5 and 1 Ga and kimberlite eruption at 240 Ma. Both datasets (plates and bulk diamond analyses) reported here cover most of the range of N content and the entire range of N aggregation previously documented



**Table 2** Averaged major element composition (EPMA results quoted in wt%) for inclusions in diamonds from Jwaneng

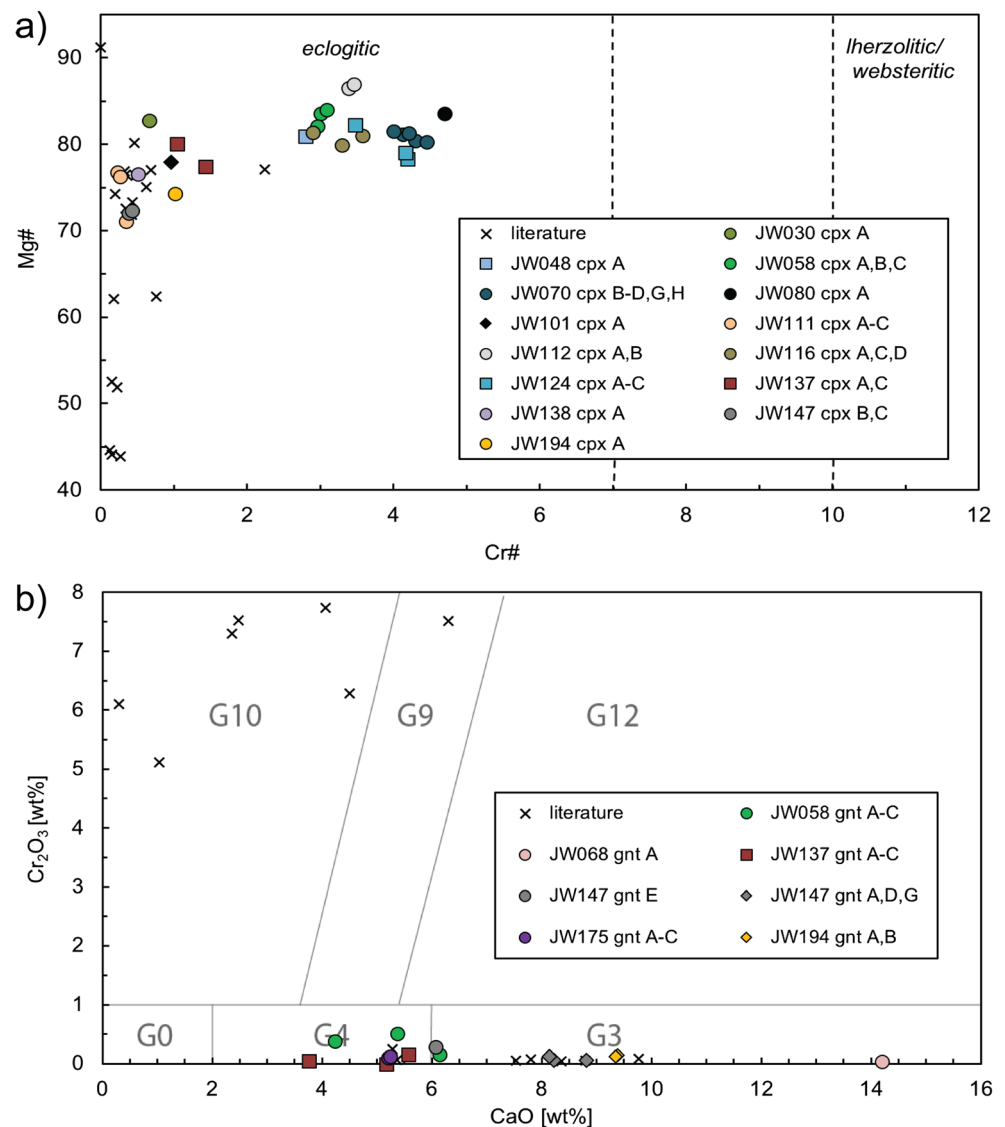
Sample	Zone*	n**	SiO <sub>2</sub>	TiO <sub>2</sub>	Al <sub>2</sub> O <sub>3</sub>	Cr <sub>2</sub> O <sub>3</sub>	FeO	MnO	MgO	CaO	NiO	Na <sub>2</sub> O	K <sub>2</sub> O	Total
JW030 cpx A	core	15	51.4	0.27	5.4	0.05	4.7	0.06	12.6	18.0	0.07	2.9	0.28	95.8
JW048 cpx A	rim	12	50.8	0.16	4.6	0.20	6.4	0.10	15.1	16.3	0.06	2.2	0.41	96.3
JW058 cpx A	core	10	52.2	0.12	5.1	0.24	5.9	0.12	16.8	13.8	0.08	2.6	0.16	97.1
JW058 cpx B	core	15	53.4	0.13	5.0	0.22	5.8	0.11	15.1	14.2	0.08	3.0	0.16	97.2
JW058 cpx C	core	9	50.2	0.13	5.2	0.25	5.9	0.11	17.3	13.9	0.08	2.3	0.16	95.5
JW070 cpx B	core	11	51.9	0.15	4.1	0.27	6.4	0.10	14.8	15.8	0.07	2.2	0.39	96.1
JW070 cpx C	core	7	54.5	0.15	3.9	0.27	6.3	0.10	14.4	16.0	0.07	2.3	0.44	98.5
JW070 cpx D	core	9	51.0	0.14	4.0	0.26	6.4	0.10	15.4	16.1	0.08	2.1	0.38	95.9
JW070 cpx G	core	10	48.5	0.15	4.0	0.26	6.3	0.10	15.4	15.8	0.07	2.2	0.42	93.3
JW070 cpx H	core	7	53.7	0.14	4.3	0.26	6.3	0.09	15.6	16.3	0.06	2.4	0.39	99.5
JW080 cpx A	core	14	54.3	0.12	3.6	0.26	5.4	0.11	15.3	16.2	0.08	2.4	0.29	98.0
JW101 cpx A	int	11	53.9	0.27	4.8	0.07	7.0	0.11	13.8	15.3	0.06	2.3	0.43	98.1
JW111 cpx A	core	12	51.5	0.41	11.9	0.04	4.5	0.04	8.4	12.3	0.02	6.4	0.09	95.7
JW111 cpx B	core	9	53.2	0.45	9.1	0.05	4.4	0.04	6.0	11.9	0.01	8.2	0.09	93.5
JW111 cpx C	core	13	52.1	0.44	12.3	0.05	4.6	0.05	8.2	12.2	0.02	5.9	0.09	95.9
JW112 cpx A	core	15	54.4	0.07	3.6	0.19	4.6	0.09	16.6	17.5	0.08	1.9	0.24	99.3
JW112 cpx B	core	12	50.1	0.07	3.6	0.19	4.6	0.08	17.0	17.2	0.08	1.9	0.25	95.0
JW116 cpx A	core	5	50.0	0.16	4.1	0.23	6.2	0.10	14.9	16.0	0.06	2.3	0.41	94.5
JW116 cpx C	core	6	50.3	0.15	4.0	0.20	6.2	0.09	13.9	15.7	0.06	2.5	0.38	93.5
JW116 cpx D	core	5	48.8	0.16	4.4	0.20	6.3	0.10	15.4	16.0	0.06	2.3	0.39	94.1
JW124 cpx A	rim	3	50.1	0.20	3.8	0.25	6.4	0.11	13.0	15.2	0.06	2.2	0.51	91.8
JW124 cpx B	rim	5	49.5	0.15	4.2	0.27	6.5	0.11	13.7	15.6	0.05	2.3	0.48	92.9
JW124 cpx C	rim	11	54.4	0.21	4.5	0.24	6.0	0.09	15.6	16.6	0.08	2.1	0.53	100.4
JW137 cpx A	rim	9	46.4	0.26	5.0	0.08	7.0	0.12	15.7	15.4	0.05	2.2	0.46	92.5
JW137 cpx C	rim	12	54.7	0.27	4.8	0.10	7.1	0.12	13.6	15.4	0.07	2.3	0.44	99.0
JW137 cpx D	rim	7	50.3	0.00	4.9	–	6.9	0.11	14.8	15.4	0.07	2.4	0.46	95.4
JW138 cpx A	core	7	51.1	0.45	10.3	0.08	5.2	0.07	9.5	13.2	0.01	5.2	0.11	95.3
JW147 cpx B	core	15	53.7	0.62	9.6	0.05	6.1	0.08	8.8	12.6	0.03	5.8	0.12	97.6
JW147 cpx C	core	11	52.6	0.59	9.6	0.06	6.2	0.07	9.1	12.8	0.05	5.6	0.13	96.8
JW194 cpx A	core	19	53.4	0.64	7.3	0.11	6.9	0.09	11.2	13.4	0.03	4.6	0.15	97.9
JW058 gnt A	core	15	35.8	0.23	23.5	0.37	12.2	0.26	19.9	4.1	0.01	0.07	0.00	96.4
JW058 gnt B	core	3	38.4	0.27	21.5	0.49	14.4	0.30	16.2	5.2	0.03	0.07	0.00	96.7
JW058 gnt C	core	14	33.7	0.70	23.3	0.15	17.9	0.33	14.3	5.9	0.00	0.16	0.00	96.5
JW068 gnt A	core	9	37.0	0.07	22.7	0.04	8.2	0.13	13.5	13.5	0.03	0.08	0.00	95.4
JW137 gnt A	rim	6	37.7	0.43	22.7	0.15	14.7	0.31	16.5	5.5	0.00	0.09	0.00	98.1
JW137 gnt B	rim	10	39.9	0.00	21.2	–	15.4	0.33	15.5	5.0	0.02	0.10	0.00	97.5
JW137 gnt C	rim?	7	40.5	0.09	20.5	0.05	16.8	0.38	15.7	3.7	0.03	0.11	0.00	97.8
JW147 gnt A	int?	14	34.1	0.71	23.2	0.05	18.8	0.33	11.0	7.9	0.01	0.19	0.00	96.4
JW147 gnt D	int?	10	36.9	0.69	21.8	0.12	19.0	0.36	10.2	7.9	0.05	0.19	0.00	97.1
JW147 gnt E	core	22	40.3	0.17	22.6	0.28	10.4	0.21	17.2	5.9	0.02	0.08	0.00	97.0
JW147 gnt G	int?	9	39.8	0.73	17.1	0.05	19.2	0.32	7.8	8.2	0.02	0.27	0.00	93.4
JW175 gnt A	core	8	30.5	0.66	22.9	0.10	20.7	0.38	13.2	4.9	0.02	0.00	0.18	93.5
JW175 gnt B	core	5	31.9	0.66	22.6	0.09	20.6	0.37	13.1	4.9	0.02	0.18	0.00	94.5
JW175 gnt C	core	5	40.8	0.73	16.4	0.12	20.5	0.37	8.1	4.8	0.04	0.25	0.00	92.2
JW194 gnt A	int	13	38.5	0.44	22.0	0.14	13.8	0.30	13.3	9.2	0.02	0.11	0.00	97.7
JW194 gnt B	int	13	42.4	0.43	19.8	0.12	13.6	0.30	11.6	9.1	0.02	0.12	0.00	97.4

\*Zone = approximate location of inclusion in core, intermediate (int) and rim zones based on visual observation only

\*\*n = number of individual analyses per grain



**Fig. 4** Molar Mg versus Cr numbers and  $\text{Cr}_2\text{O}_3$  versus CaO (in wt%) of diamond inclusions from Jwaneng. **a)** The 30 liberated omphacite (cpx) inclusions are compared to literature data from Richardson et al. (2004) in a clinopyroxene classification diagram after Stachel and Harris (2008). The inclusion data show 2 compositional subgroups, one with low-Cr# around 1.0 from diamond growth zones with  $\geq 50$  at.ppm N and a second with high-Cr# between 3 and 4 from growth zones with N generally  $\leq 50$  at.ppm. **b)** The 15 liberated pyrope-almandine (gnt) inclusions are compared to literature data from Richardson et al. (1999, 2004) and Stachel et al. (2004) in a garnet classification diagram after Grütter et al. (2004). The inclusion data show 2 compositional subgroups with garnets from growth zones with low N contents ( $\leq 50$  at.ppm) having low-Ca (G4), except for JW175 (1000 at.ppm N), while garnet inclusions from growth zones with higher N contents (50 to 200 at.ppm) also have higher Ca-contents (G3). Coloured symbols are subdivided based on the location of an inclusion in the host diamond: core zone (filled circle), intermediate (diamond) and rim (square)



this study and the literature provide broad insights into the N characteristics of the prevalent diamond populations (Online Resources ESM 6), this approach averages the significant N concentration variation found in diamonds that record multiple growth events and systematically overestimates the N aggregation.

Further information on growth relationships between Jwaneng diamonds and their eclogitic inclusions can be found in a complementary study of Davies et al. (2018). The diamonds of that study were also sampled during the campaign at DTC.

### Peridotitic diamonds

Deines et al. (1997) state that peridotitic diamonds ( $n = 20$ ) tend to have lower N contents compared to the eclogitic suite but are similar in N aggregation state and postulate 3 different

growth environments for olivine-bearing diamonds based on N-content, C-isotopes and mineral composition. We make similar observations based on the FTIR data from the eight studied peridotitic plates with 2 that are pure Type IIa, 4 that include Type IIa growth zones and 2 with 330 to 760 at.ppm N and highly variable aggregation; 0–88 %B. The combined CL and FTIR characteristics of the individual peridotitic diamonds establish that they were formed in a single growth event (e.g., JW020, Fig. 3) or contain 2 (e.g., JW243, Fig. 2j & Fig. 3) to 3 (e.g., JW102, Fig. 2i & Fig. 3) distinct growth zones that record changes in modelled residence temperatures of several tens of degrees from core to rim. Clearly, an expanded sample set and detailed chronology of these growth zones is required to establish the intervals between individual growth zones and whether the timescale of P-type diamond growth is comparable to that of the more common E-type diamonds or distinct as suggested by Stachel et al. (2004).

## Eclogitic diamonds

By combining the N-characteristics obtained from FTIR with the CL imagery of diamond plates, the Jwaneng diamonds are seen to represent a highly varied population. Five samples that exhibit multiple growth zones plot along a single isotherm (e.g., JW083, JW455, JW94, JW196, JW210 in Fig. 3). As the different growth zones of individual diamonds exhibit a near constant thermal history, this suggests that these individual diamonds were formed by pulses of fluid in a single diamond-forming event or formed within a short period of time (100's Myr, i.e. the effective resolution obtained in Fig. 3). Samples JW044 (Fig. 2b) and JW058 also potentially formed in a single event. In contrast, the majority (>90%) of the eclogitic diamond plates record 2 (e.g., JW111, Fig. 2e; JW047; Fig. 2h), 3 (e.g., JW024, Fig. 2g; JW060, Fig. 2k) or 4 (e.g., JW033, Fig. 2d; JW194, Fig. 2l) changes in modelled mantle residence temperatures, ranging from 10s of °C (JW024) to >100 °C (e.g., JW033, JW111, JW175, JW194; Fig. 3), between individual growth zones of single diamonds. Assuming near-constant temperatures throughout the whole residence period, the cores of these plates typically show higher N aggregation compared to the rims, which most probably implies that there is a significant time gap between growth of the core and rim. If the core experienced a hotter period of residence prior to rim formation, this inferred time gap decreases. In principle, there is an indefinite number of combinations of time and temperature possible if the corresponding inclusion ages are unknown. Hence, accurate dates for individual growth zones (i.e. core and rim) are required to more accurately model their residence temperatures (Kohn et al. 2016) and to constrain the time gap between individual growth zones. In a few cases there also appears to be evidence for higher model temperatures in diamond rims (JW003, JW030, JW045). This cannot be correct, as the cores must be at least as old the rims and any high temperature event experienced by the rim would also have been experienced by the core. The most likely explanation to these observations are modelled temperature anomalies resulting from overlapping zones (Kohn et al. 2016). Other possible explanations may include a deviation from the expected kinetics of A to B centre aggregation, perhaps caused by some additional defect incorporation (e.g., see Fisher and Lawson (1998) for the effect of Ni and Co on N-aggregation in diamond).

The presence of different inclusion populations in diamonds of distinct N contents is interpreted to record modifications in the lithospheric mantle beneath the Kaapvaal Craton involving different metasomatic fluids. Omphacites with low Mg# and Cr# and high-Ca pyrope-almandines (Fig. 4) are included in diamond growth zones with 50 to 700 at.ppm N whereas omphacites with high Mg# and Cr# and low-Ca pyrope-almandines come from diamond growth zones with low N (generally  $\leq 50$  at.ppm). The data from these inclusions

suggests that either the original mantle protoliths have different C-buffering capacities or that fluids of different composition metasomatized the lithosphere at different depths and, potentially, times. This may explain why JW175 has high N contents (1000 at.ppm) although the garnets are low-Ca pyrope-almandines. The interpretation of multiple diamond forming events is consistent with observations based on coexisting garnet and clinopyroxene equilibration temperatures and FTIR data described in Deines et al. (1997) as well as the inclusion dating studies of Richardson et al. (1999, 2004) that argued for diamond formation at 2.9, 1.5 and 1.0 Ga.

We conclude that our FTIR dataset is very useful in revealing the varied time-temperature characteristics of a diamond population, but that either temperature or age constraints from inclusion studies are required for a robust and quantitative interpretation. The dataset emphasizes the complex growth histories recorded by the diamond suite. The record of up to 4 distinct growth zones in single silicate inclusion-bearing diamonds (JW033, Fig. 2d; JW194, Fig. 2l; Fig. 3) requires further chronology to establish the time intervals between the genesis of these individual zones. Such data would also allow for more rigorous interpretation of the FTIR dataset to determine whether the diamond populations reflect a few large-scale diamond-forming events (i.e. samples of the same age with varied thermal histories, indicating diamond growth over a significant depth profile of the mantle), or alternatively more frequent diamond formation on a much smaller, local scale as a result of confined movements of metasomatic fluids.

## Conclusion

The data from this study support five main conclusions. (i) Counting statistics for 130,000 diamonds from Jwaneng emphasise the predominance of an overwhelming (>88%) eclogitic diamond suite with individual production parcels containing up to 10% inclusion-bearing diamonds (5% on average). (ii) Over 80% of the eclogitic and peridotitic diamond plates record changing FTIR characteristics with 2, 3 or 4 individual growth zones potentially spanning extended timescales during the evolution of the Kaapvaal Craton, while a minority of inclusion-bearing diamonds were likely formed in a single event. This observation has not been quantified for inclusion-free diamonds. (iii) FTIR data acquired for bulk diamonds integrate N defects from multiple growth zones and consequently do not record the total internal variability, especially when major changes between individual growth zones are present. (iv) Two compositional subgroups of eclogitic garnet and cpx inclusions with different characteristics in N content of their diamond hosts were identified and imply different diamond forming conditions (i.e. a combination of different protoliths, formation depth, fluid composition

and most probably age). (v) Detailed examination of diamond plates by CL imaging and FTIR identifies at least 7 individual diamond-forming events recorded in peridotitic (3) and eclogitic (4) diamonds. The scale and timing between these individual events is yet to be fully resolved, as is their distribution with depth.

**Acknowledgements** The authors sincerely thank Debswana and De Beers for providing access to run of mine production at DTCB and the generous supply of diamonds. Special thank goes to Samantha H. Perritt, Suzette Timmerman, Cas Nooitgedacht, Evalien A.S. van der Valk and Siem Peters who helped with the counting statistics, as well as the members of the Diamond Damage Management Department (DDMD) Tebogo Masire, Keletso Taolo and Robert Phiri accommodating us at DTCB and Onameditse Keitebetse for arranging the sample export. Travel for sampling was sponsored by Stichting Dr. Schurmannfonds. Thomas Stachel is thanked for providing access to the DeBeers Diamond Laboratory in Edmonton for FTIR analyses and to the diamond inclusion database, Sergei Matveev and Peter van Krieken for support with FTIR and EPMA in Utrecht, Frank J.C. Peeters for providing access to the EDF microscopy, Pieter Ouwerkerk and Gassan Diamonds BV for assistance in polishing. The manuscript benefitted from constructive comments of Fanus Viljoen, an anonymous expert, and editor Thomas Stachel.

**Open Access** This article is distributed under the terms of the Creative Commons Attribution 4.0 International License (<http://creativecommons.org/licenses/by/4.0/>), which permits unrestricted use, distribution, and reproduction in any medium, provided you give appropriate credit to the original author(s) and the source, provide a link to the Creative Commons license, and indicate if changes were made.

## References

- Boyd S, Kiflawi I, Woods G (1994) The relationship between infrared absorption and the A defect concentration in diamond. *Philos Mag B* 69:1149–1153
- Boyd S, Kiflawi I, Woods G (1995) Infrared absorption by the B nitrogen aggregate in diamond. *Philos Mag B* 72:351–361
- Cartigny P, Harris JW, Javoy M (1998) Eclogitic diamond formation at Jwaneng: no room for a recycled component. *Science* 280:1421–1424
- Davies GR, van den Heuvel Q, Matveev S, Drury MR, Chinn IL, Gress MU (2018) A combined cathodoluminescence and electron backscatter diffraction examination of the growth relationships between Jwaneng diamonds to their inclusions (in this issue)
- Deines P, Harris JW, Gurney JJ (1997) Carbon isotope ratios, nitrogen content and aggregation state, and inclusion chemistry of diamonds from Jwaneng, Botswana. *Geochim Cosmochim Acta* 61:3993–4005
- Fisher D, Lawson SC (1998) The effect of nickel and cobalt on the aggregation of nitrogen in diamond. *Diam Relat Mater* 7:299–304
- Grütter HS, Gurney JJ, Menzies AH, Winter F (2004) An updated classification scheme for mantle-derived garnet, for use by diamond explorers. *Lithos* 77:841–857
- Gurney J, Harris J, Otter M, Rickard R (1995) Jwaneng diamond inclusions. In: 6th International Kimberlite Conference, pp 208–210
- Gurney JJ, Hildebrand PR, Carlson JA, Fedortchouk Y, Dyck DR (2004) The morphological characteristics of diamonds from the Ekati property, Northwest Territories, Canada. *Lithos* 77:21–38
- Howell D, O'Neill C, Grant K, Griffin W, Pearson N, O'Reilly S (2012a)  $\mu$ -FTIR mapping: distribution of impurities in different types of diamond growth. *Diam Relat Mater* 29:29–36
- Howell D, O'Neill C, Grant K, Griffin W, O'Reilly S, Pearson N, Stern R, Stachel T (2012b) Platelet development in cuboid diamonds: insights from micro-FTIR mapping. *Contrib Mineral Petr* 164:1011–1025
- Kinny P, Compston W, Bristow J, Williams I (1989) Archaean mantle xenocrysts in a Permian kimberlite: 2 generations of kimberlitic zircon in Jwaneng DK2, southern Botswana. *Kimberlites and Related Rocks* 2:833–842
- Kohn SC, Speich L, Smith CB, Bulanova GP (2016) FTIR thermochronometry of natural diamonds: A closer look. *Lithos* 265:148–158
- Koornneef JM, Gress MU, Chinn IL, Jelsma HA, Harris JW, Davies GR (2017) Archaean and Proterozoic diamond growth from contrasting styles of large-scale magmatism. *Nat Commun* 8:648
- Leahy K, Taylor W (1997) The influence of the Glennie domain deep structure on the diamonds in Saskatchewan kimberlites. *Geol Geofiz* 38:451–460
- Pearson D, Shirey S, Harris J, Carlson R (1998) Sulphide inclusions in diamonds from the Koffiefontein kimberlite, S Africa: constraints on diamond ages and mantle Re–Os systematics. *Earth Planet Sc Lett* 160:311–326
- Richardson SH, Chinn IL, Harris JW (1999) Age and origin of eclogitic diamonds from the Jwaneng kimberlite, Botswana. The PH Nixon Volume Proceedings of the Seventh International Kimberlite Conference, Cape Town Red Roof Design, Cape Town.,:734–736
- Richardson SH, Shirey SB, Harris JW (2004) Episodic diamond genesis at Jwaneng, Botswana, and implications for Kaapvaal craton evolution. *Lithos* 77:143–154
- Smith C, Gurney J, Harris J, Otter M, Kirkley M, Jagoutz E (1991) Neodymium and strontium isotope systematics of eclogite and websterite paragenesis inclusions from single diamonds, Finsch and Kimberley Pool, RSA. *Geochim Cosmochim Acta* 55:2579–2590
- Speich L, Kohn SC, Wirth R, Bulanova GP, Smith CB (2017) The relationship between platelet size and the B' infrared peak of natural diamonds revisited. *Lithos* 278–281:419–426
- Stachel T, Harris JW (2008) The origin of cratonic diamonds — constraints from mineral inclusions. *Ore Geol Rev* 34:5–32
- Stachel T, Viljoen KS, McDade P, Harris JW (2004) Diamondiferous lithospheric roots along the western margin of the Kalahari Craton—the peridotitic inclusion suite in diamonds from Orapa and Jwaneng. *Contrib Mineral Petr* 147:32–47
- Thomassot E, Cartigny P, Harris J, Lorand J, Rollion-Bard C, Chaussidon M (2009) Metasomatic diamond growth: a multi-isotope study (13 C, 15 N, 33 S, 34 S) of sulphide inclusions and their host diamonds from Jwaneng (Botswana). *Earth Planet Sc Lett* 282:79–90
- Timmerman S, Matveev S, Gress MU, Davies GR (2015) A methodology for wavelength dispersive electron probe microanalysis of unpolished silicate minerals. *J Geochem Explor* 159:243–251
- Timmerman S, Koornneef JM, Chinn IL, Davies GR (2017) Dated eclogitic diamond growth zones reveal variable recycling of crustal carbon through time. *Earth Planet Sc Lett* 463:178–188
- Wiggers de Vries D, Pearson D, Bulanova G, Smelov A, Pavlushin A, Davies G (2013) Re–Os dating of sulphide inclusions zonally distributed in single Yakutian diamonds: evidence for multiple episodes of Proterozoic formation and protracted timescales of diamond growth. *Geochim Cosmochim Acta* 120:363–394